PCCP

PAPER

View Article Online
View Journal | View Issue

Cite this: *Phys. Chem. Chem. Phys.*, 2023, **25**, 21416

Heterogenised catalysts for the H-transfer reduction reaction of aldehydes: influence of solvent and solvation effects on reaction performances†

Atika Muhammad,‡[a] Chengxu Zhu,‡[a] Xiao Yu,[a] Graziano Di Carmine,[b] Hannah Wood,[a] Paola Carbone,[a] Sam P. de Visser,[a] Christopher Hardacre[a] and Carmine D'Agostino *[ac]

Heterogenisation of homogeneous catalysts onto solid supports represents a potential strategy to make the homogeneous catalytic function recyclable and reuseable. Yet, it is usually the case that immobilised catalysts have much lower catalytic activity than their homogeneous counterpart. In addition, the presence of a solid interface introduces a higher degree of complexity by modulating solid/fluid interactions, which can often influence adsorption properties of solvents and reactive species and, ultimately, catalytic activity. In this work, the influence of support and solvent in the H-transfer reduction of propionaldehyde over $Al(O^iPr)_3$–SiO_2, $Al(O^iPr)_3$–TiO_2 and $Al(O^iPr)_3$–Al_2O_3 heterogenised catalysts has been studied. Reaction studies are coupled with both NMR relaxation measurements as well as molecular dynamics (MD) simulations in order to unravel surface and solvation effects during the reaction. The results show that, whilst the choice of the support does not influence significantly catalytic activity, reactions carried out in solvents with high affinity for the catalyst surface, or able to hinder access to active sites due to solvation effects, have a lower activity. MD calculations provide key insights into bulk solvation effects involved in such reactions, which are thought to play an important role in determining the catalytic behaviour. The activity of the heterogenised catalysts was found to be comparable with that of the homogeneous $Al(O^iPr)_3$ catalysts for all supports used, showing that for the type of reaction studied immobilisation of the homogeneous catalyst onto solid supports is a viable, robust and effective strategy.

Received 20th April 2023,
Accepted 4th July 2023

DOI: 10.1039/d3cp01825c

rsc.li/pccp

1. Introduction

Manufacturing of fine chemicals through catalysis is a very active area of research, with applications in the food, fragrance, cosmetic and pharmaceutical industries. For such processes, homogeneous catalysts, which typically have metal centres surrounded by a variety of ligands, are extremely flexible, function at mild conditions, and can provide exceptionally high selectivity.[1] Major drawbacks of homogeneous catalysis are the difficulty in separating and reusing the catalyst, as well as the need for using batch processes, which are more suitable with such catalysts. Moreover, reactions catalysed by homogeneous catalysts can be highly cost ineffective due to the requirement for catalyst replacement and related waste disposal. Conversely, heterogeneous catalysts, which are often made of metal particles supported on porous solid or metal oxides, offer practical advantages in terms of separation from the reaction products and process operability but tend to work at harsher conditions and with lower conversion and selectivity.[2–4] A possible strategy to carry out processes having the advantages of both heterogeneous and homogeneous catalysis is that of immobilising homogeneous catalytic functions over solid supports, hence making the catalyst insoluble and easy to recover or be integrated in continuous fixed-bed reactors.[5,6] The functionalisation of homogeneous catalysts can be achieved by grafting processes.[7,8] In this method, the support is usually suspended in a solvent under reflux and reacted with an appropriate loading of a suitable homogeneous catalyst precursor.[8] The resulting solid is collected, washed and dried in order to obtain the final heterogenised homogeneous catalyst. The nature of the support material

[a] *Department of Chemical Engineering, The University of Manchester, Oxford Road, M13 9PL, UK. E-mail: carmine.dagostino@manchester.ac.uk*
[b] *Dipartimento di Scienze Chimiche, Farmaceutiche ed Agrarie, Università degli Studi di Ferrara, Via L. Borsari, 46, I-44121 Ferrara, Italy*
[c] *Dipartimento di Ingegneria Civile, Chimica, Ambientale e dei Materiali (DICAM), Alma Mater Studiorum – Università di Bologna, Via Terracini, 28, 40131 Bologna, Italy*

† Electronic supplementary information (ESI) available. See DOI: https://doi.org/10.1039/d3cp01825c

‡ These two authors contributed equally to this work and are co-first authors.

may have a significant impact on the catalyst behaviour and influence the catalyst active site.[9] The choice of supports with high surface area for absorption, good thermal stability and porosity is highly recommended. Among the supports, silica (SiO_2)-based supports are the most commonly used. We have recently demonstrated that the use of other supports, such as TiO_2 and Al_2O_3, can also be a valid alternative to produce highly active and selective catalysts for immobilising aluminium isopropoxide to catalyse H-transfer reductions of carbonyl compounds.[10] H-transfer reactions are very useful for the selective reduction of carbonyl compounds to their corresponding alcohols and are traditionally carried out in homogeneous solutions using soluble metal alkoxides.[11,12] The alkoxides required are often in stoichiometric quantities and cannot be recycled. This results in high volumes of corrosive waste and possibilities of side reactions, such as aldol condensation.[13] Previous work has shown that H-transfer reactions can be catalysed using solid catalysts. Heterogeneous catalysts, such as zeolites, magnesium phosphates, CaO and MgO_x/Al_2O_3, have been used for this reaction under mild conditions.[4,14] However, they typically have poor selectivity and the catalysts are difficult to tune. In addition to heterogeneous catalysts, metal alkoxides have also been immobilised on silica based supports to be used for H-transfer reactions. Uysal and Oksal reported the activity of boron alkoxide containing ordered mesoporous silica ($B(O^iPr)_3$-MCM-41) prepared by grafting method for the reduction of α,β-unsaturated carbonyl compounds.[15] They found the catalyst to be very selective without leaching of the grafted boron.[15] Zhu *et al.* also used SBA-15 as a support material for the grafting of zirconium 1-propoxide.[16] They found the supported catalyst to be very active in H-transfer reduction of various aldehydes and ketones. MCM-41 material was also employed by Anwander *et al.* as a support for the grafting of aluminium isopropoxide.[13] It was found that the supported catalyst was particularly active in the H-transfer reduction of 4-*tert*-butylcyclohexanone. However, despite their potential, heterogeneous systems have received far less attention relatively to homogeneous systems due to several issues. For example, mass transfer effects by diffusion[17,18] and competitive adsorption[19] are some of the factors that can affect the performance of heterogeneous catalysts due to the presence of a porous solid support. NMR techniques to measure transport and dynamics in fluid systems[20–22] have in recent years been successfully applied to study heterogeneous catalysts. In particular, NMR relaxation studies have recently been used to investigate adsorption on solid catalysts[23–27] and aid design of heterogeneous catalytic systems.[28] In particular, the ratio of T_1/T_2 has previously been used as an indicator of surface–molecule interaction energy in porous materials, as it correlates with the residence time of the molecule on the surface.[25] Under certain conditions, a high T_1/T_2 ratio indicates stronger molecule–surface interactions.

Following our previous investigation on the effect of the type of support for immobilisation of aluminium isopropoxide,[10] in this work we have extended our approach for H-transfer reduction of carbonyl compounds through immobilised organometallic aluminium isopropoxide. In particular, we assess solvent and solvation effects, gaining new fundamental insights at a molecular level through NMR relaxation measurements to probe solvent effects over the surface, and molecular dynamics (MD) to probe bulk solvation effects that might affect the reaction pathway.

2. Experimental

2.1. Materials and chemicals

Aluminium isopropoxide (>98%), 2-propanol (anhydrous, 99.5%), *n*-hexane (anhydrous, >99%) 1,4-dioxane (anhydrous, 99.8%), diethyl ether (>98%), titanium(IV) oxide (anatase) and silica were obtained from Sigma Aldrich, UK. Toluene (99.5%) and propionaldehyde (extra pure, SLR) were obtained from Fisher Scientific UK, while cyclohexane (99%) was purchased from Acros and aluminium oxide, γ-phase, from Alfa Aesar.

2.2. Preparation of supported catalysts

The grafting of aluminium isopropoxide $Al(O^iPr)_3$ on the various supports was carried out in accordance with the literature.[29] Before grafting, the support (SiO_2, TiO_2, γ-Al_2O_3) was dried for 4 hours at a temperature of 250 °C. The heterogenised homogenous catalyst was prepared by adding 2 g of the support (SiO_2, TiO_2, γ-Al_2O_3) to a solution of (5 mmol) aluminium isopropoxide in 25 ml dry *n*-hexane. The solution was stirred (500–700 rpm) and refluxed at 69 °C for 12 hours. The suspension was filtered under N_2 atmosphere, washed three times with *n*-hexane and dried under the same inert condition.

2.3. Reaction studies

The heterogenised catalysts $Al(O^iPr)_3$–SiO_2, $Al(O^iPr)_3$–TiO_2 and $Al(O^iPr)_3$–Al_2O_3 were tested for the H-transfer reduction of propionaldehyde to 1-propanol using 2-propanol as sacrificial H-donor agent. Reactions were carried out in a 50 ml round-bottom flask equipped with a condenser that was submerged in an oil bath. The heterogenised catalyst (200–220 mg) was added to the reaction mixture containing 1.4 mmol propionaldehyde, 6.6 mmol 2-propanol and the solvent of interest (5 ml). The reaction mixture was then heated to reflux with stirring at 750 rpm for 4 hours. The mixture was analysed using an Agilent 7820A gas chromatography system equipped with FID detector and a HP-5 methylpolysiloxane column (30 m × 320 μm × 0.25 μm), operated at 35 °C for 5 minutes, heating at 10 °C minute^{-1} up to 200 °C for 16 minutes. Products were identified by comparison with authentic samples and quantified by external calibration method. The main product was 1-propanol for all catalysts and solvents.

The turnover frequency (TOF) was determined using the expression:

$$\mathrm{TOF} = \frac{\mathrm{mmol_{product}}}{\mathrm{mmol_{catalyst}} \times \mathrm{time(s)}}$$

2.4. NMR relaxation measurements

Proton (^{1}H) NMR measurements were conducted using a Magritek Spinsolve 43 MHz NMR spectrometer. For the sample preparation, catalyst particles were soaked in the solvent or reactant of interest for 48 hours to enable saturation.

The samples were then dried on a pre-soaked filter paper to eliminate any surplus liquid on the external surface. After carefully transferring the powder samples into a 5 mm diameter NMR tube, a small amount of the solvent or reactant was adsorbed onto filter paper. This filter paper was then placed underneath the cap of the NMR tube and sealed with Parafilm to create a saturated atmosphere in the NMR tube, minimising errors caused by the evaporation of the volatile liquids. Standard inversion recovery pulse sequence was used to measure T_1. More details on pulse sequence and data analysis can be found in the literature.[30] General parameters for T_1 measurements are a repetition time of 20 s; min delay 1–250 ms; max delay 1–15 s; dwell time 50 μs. The Carr Purcell Meiboom Gill (CPMG) pulse sequence was used to measure the transverse relaxation time, T_2.[30] General parameters for T_2 measurements were a repetition time of 10 s; echo time 1000 μs; number of echoes per step 20–250; number of steps 16; number of scans 4; dwell time 50 μs. Before beginning the measurements, the samples were inserted into the magnet and left for about 20 minutes to attain equilibrium temperature.

2.5. Molecular dynamics simulations

Molecular dynamics (MD) simulations were carried out to understand bulk solvation effects in the MPV reduction. The MD simulations were performed using the GROMACS 2020 software package[31,32] and the General Amber Force Field (GAFF).[33] Here, parameter information, including bond, angle, torsion, improper, van der Waals, and electrostatic terms of the catalyst aluminium isopropoxide, were generated by the Metal Center Parameter Builder (MCPB.py).[34] More specifically, the organometallic compound was split into 4 residues (3 ligands and a metal ion Al), and then MCPB.py was used to generate parameters at the B3LYP/TZVP with GD3BJ dispersion correction level using Gaussian16[35] and partial charges using restrained electrostatic potential charges (RESP).[36] All topology and coordinate files were created by the TLeap module in AMBER 20 software package.[37] The AMBER-style input files were then converted to GROMACS-style using the ParmEd program in AmberTools21.[38] GAFF parameters are shown in Table S1 (ESI†). Parameters for each component in the calculation, including five solvents, one catalyst and two reactants, are presented in Tables S2–S9 (ESI†).

The simulations were performed in five cubic boxes to which periodic boundary conditions were applied in all directions. The initial systems were built using PACKMOL (version 18.104).[39] The reactants (propionaldehyde and 2-propanol), the catalyst aluminium isopropoxide, and one of the solvent types (cyclohexane, diethyl ether, 1,4-dioxane, *n*-hexane and toluene) were initially placed randomly in a $5 \times 5 \times 5$ nm^3 cubic box. The number of molecules in simulations are presented in Table 1. The simulation box dimensions of different systems after *NPT* equilibration are also shown in this table. All systems were initially minimised using the steepest descent energy minimisation method and then simulated for 1 ns at 298.15 K under the canonical (*NVT*) ensemble to reach equilibrium. The temperature was controlled with a velocity-rescaling thermostat with a coupling constant of 0.1 ps.[40] The systems were then further equilibrated for 5 ns under the isothermal–isobaric (*NPT*) ensemble with temperature maintained at 298.15 K using a velocity-rescaling thermostat and pressure at 1 bar using Parrinello–Rahman barostat;[41] a coupling constant of 0.1 ps was applied for both temperature and pressure. The equilibrium steps were followed by a 50 ns *NPT* production run, keeping temperature and pressure constant at 298.15 K and 1 bar, respectively. In all simulations, the short range electrostatic and van der Waals interactions were evaluated with a cutoff distance of 1.0 nm. Long-range electrostatic interactions were calculated using the Particle Mesh Ewald (PME) method[42] with a grid spacing of 0.16 Å. Bonds involving H were constrained to equilibrium length by applying the LINCS algorithm.[43] Analysis was performed using tools provided in the GROMACS package. Fig. 1 presents a visualisation of the cyclohexane system after a 50 ns simulation using Visual Molecular Dynamics (VMD)[44] and PyMOL (The PyMOL Molecular Graphics System, ver. 2.4; Schrödinger, LLC, 2020).

3. Results and discussion

3.1. Activity of the heterogenised *vs.* homogeneous Al(O^{i}Pr)$_3$ catalysts

The H-transfer reduction of propionaldehyde to isopropanol was chosen as a model reaction. As previously reported with the homogeneous aluminium alkoxide catalyst,[45] the reaction was carried out in a similar manner using the developed heterogenised catalysts. Detailed characterisation of these samples has been reported in previous work.[10] The specific surface area determined by Brunauer–Emmett–Teller (BET) method is in the range of 12–14 m^2 g^{-1} for Al(O^{i}Pr)$_3$–TiO$_2$ and TiO$_2$ support, 212–240 m^2 g^{-1} for Al(O^{i}Pr)$_3$–Al$_2$O$_3$ and γ-Al$_2$O$_3$ and 408–434 m^2 g^{-1} for Al(O^{i}Pr)$_3$–SiO$_2$ and SiO$_2$, while the pore size, determined by the Barrett–Joyner–Halenda (BJH) analysis, is in the range of 3–12 nm. X-ray diffraction measurements (XRD) on these catalysts shows that the homogeneous aluminium isopropoxide catalyst is highly dispersed on the surface of the supports as no new peaks of Al were detected. The high

Table 1 Number of molecules of each substance and size of simulation boxes used for MD simulations

System	Aluminium isopropoxide	Solvent	Propionaldehyde	2-Propanol	Total no. of molecules	Box size [nm^3]
Cyclohexane	7	478	54	241	780	5.05325^3
Diethyl ether	7	502	53	234	796	4.99356^3
1,4-Dioxane	6	646	46	204	902	4.93890^3
n-Hexane	8	367	62	274	711	5.02370^3
Toluene	7	488	54	238	787	5.02973^3

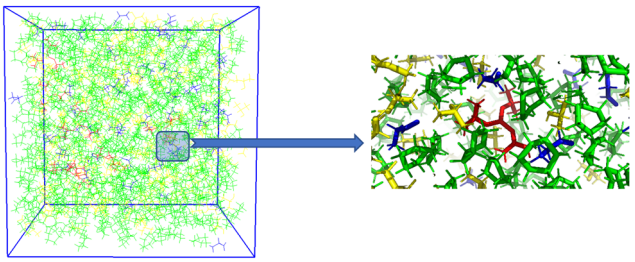

Fig. 1 Visualisation of solvent effects in a cyclohexane box. (aluminium isopropoxide: red; cyclohexane: green; 2-propanol: yellow; propionaldehyde: blue. All molecules are drawn in line style).

dispersion of Al is confirmed by the elemental dispersive X-ray spectroscopy (EDX) analysis of the samples, which shows presence of Al and C in the heterogenised catalysts.

The aluminium loading determined by ICP-OES is approximately 6.61 wt%, 5.99 wt% and 6.45 wt% for $Al(O^iPr)_3$–SiO_2, $Al(O^iPr)_3$–TiO_2 and $Al(O^iPr)_3$–Al_2O_3, respectively. To compare the catalytic activity of the heterogenised catalysts with that of the homogeneous catalysts, the TOF of for both homogenous and the heterogenised reactions are presented in Table 2.

As can be observed from Table 2, the activity of the heterogenised catalysts ($Al(O^iPr)_3$–SiO_2, $Al(O^iPr)_3$–TiO_2 and $Al(O^iPr)_3$–Al_2O_3) in different solvents is noteworthy as it compares well with that of the homogeneous aluminium isopropoxide catalyst ($Al(O^iPr)_3$). The observation that these heterogenised systems perform as well as the relevant homogeneous catalyst is unusual. In many cases heterogenisation of homogeneous catalysts often leads to a much lower activity compared to the homogeneous system.[46] In addition, it is noted that the choice of the catalyst support does not significantly affect the catalytic activity, with catalysts based on SiO_2 and γ-Al_2O_3 giving comparable performance while TiO_2 showing a slightly lower catalytic activity as shown in Fig. 2. This small change may be attributable to the lower surface area of the TiO_2 support, which can affect the aluminium isopropoxide dispersion.

Table 2 TOF values for the H-transfer reduction of propionaldehyde to 1-propanol using homogeneous and heterogenised catalysts in different solvents

Entry	Catalyst	Solvent	TOF [s^{-1}]
1.	$Al(O^iPr)_3$	*n*-Hexane	1.95×10^{-4}
2.	$Al(O^iPr)_3$–SiO_2	*n*-Hexane	1.74×10^{-4}
3.	$Al(O^iPr)_3$–TiO_2	*n*-Hexane	1.62×10^{-4}
4.	$Al(O^iPr)_3$–Al_2O_3	*n*-Hexane	1.69×10^{-4}
5.	$Al(O^iPr)_3$	Cyclohexane	1.89×10^{-4}
6.	$Al(O^iPr)_3$–SiO_2	Cyclohexane	1.44×10^{-4}
7.	$Al(O^iPr)_3$–TiO_2	Cyclohexane	1.35×10^{-4}
8.	$Al(O^iPr)_3$–Al_2O_3	Cyclohexane	1.43×10^{-4}
9.	$Al(O^iPr)_3$	Toluene	1.65×10^{-4}
10.	$Al(O^iPr)_3$–SiO_2	Toluene	1.17×10^{-4}
11.	$Al(O^iPr)_3$–TiO_2	Toluene	1.10×10^{-4}
12.	$Al(O^iPr)_3$–Al_2O_3	Toluene	1.12×10^{-4}
13.	$Al(O^iPr)_3$	1,4-Dioxane	9.79×10^{-5}
14.	$Al(O^iPr)_3$–SiO_2	1,4-Dioxane	7.22×10^{-5}
15.	$Al(O^iPr)_3$–TiO_2	1,4-Dioxane	6.94×10^{-5}
16.	$Al(O^iPr)_3$–Al_2O_3	1,4-Dioxane	7.08×10^{-5}
17.	$Al(O^iPr)_3$	Diethyl ether	6.67×10^{-5}
18.	$Al(O^iPr)_3$–SiO_2	Diethyl ether	6.53×10^{-5}
19.	$Al(O^iPr)_3$–TiO_2	Diethyl ether	5.97×10^{-5}
20.	$Al(O^iPr)_3$–Al_2O_3	Diethyl ether	6.39×10^{-5}

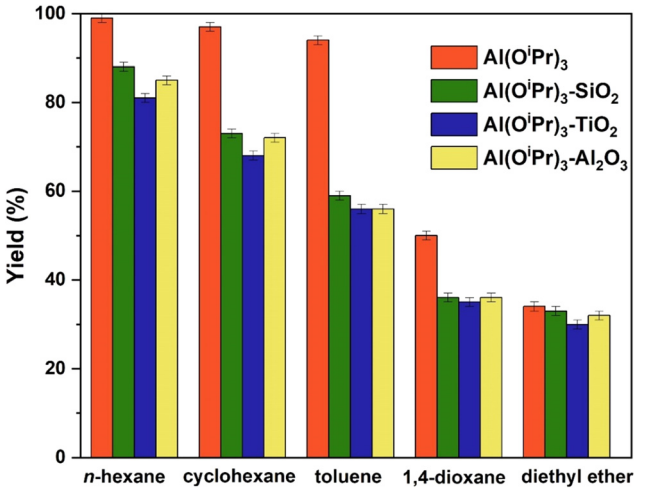

Fig. 2 Yields of 1-propanol in different solvents for the heterogenised catalysts.

3.2. Solvent effects in the heterogenised catalysts

After having explored the effect of the support used for the immobilisation of the aluminium active species, we now turn our attention to the influence of the choice of the solvent. Fig. 2 shows the yields of the various heterogenised catalysts in different solvents. It can be observed that the differences in the yield are similar to those reported using the homogeneous aluminium isopropoxide (as shown in Table 2). The yields are significantly lower in 1,4-dioxane and diethyl ether solvents compared to toluene, cyclohexane and aliphatic *n*-hexane. It is clear by looking at the Kamlet and Taft parameters[47,48] that solvents with high hydrogen bonding ability and high polarizability, such as 1,4-dioxane and diethyl ether show reduced activity. This suggests the possibility of the solvents coordinating with the aluminium centre to block access of the reactant to the active sites of the catalysts. The best performance of the heterogenised catalysts is observed when using aprotic solvents (*n*-hexane and cyclohexane). The trend observed for the supported aluminium catalyst with the type of solvent is similar to that observed for homogeneous aluminium isopropoxide. This suggests that for the effects related to the stabilisation of transition state as well as solvation effects observed for the homogeneous catalyst play a similar role when the active catalyst is immobilised over the support.

In order to probe the solvent effects in more detail, for example the influence of solvent adsorption over the solid surface of the heterogenised catalysts, NMR relaxation experiments were conducted to elucidate solvent–surface interaction. In particular, the T_1/T_2 ratio can be considered as an indicator characterising the strength of fluid/solid interaction at the surface.[25] In more details, a higher T_1/T_2 ratio of fluids inside porous materials results from a slower molecular dynamics of molecules close to the surface interacting with the solid. In summary, a higher T_1/T_2 can be attributed to stronger

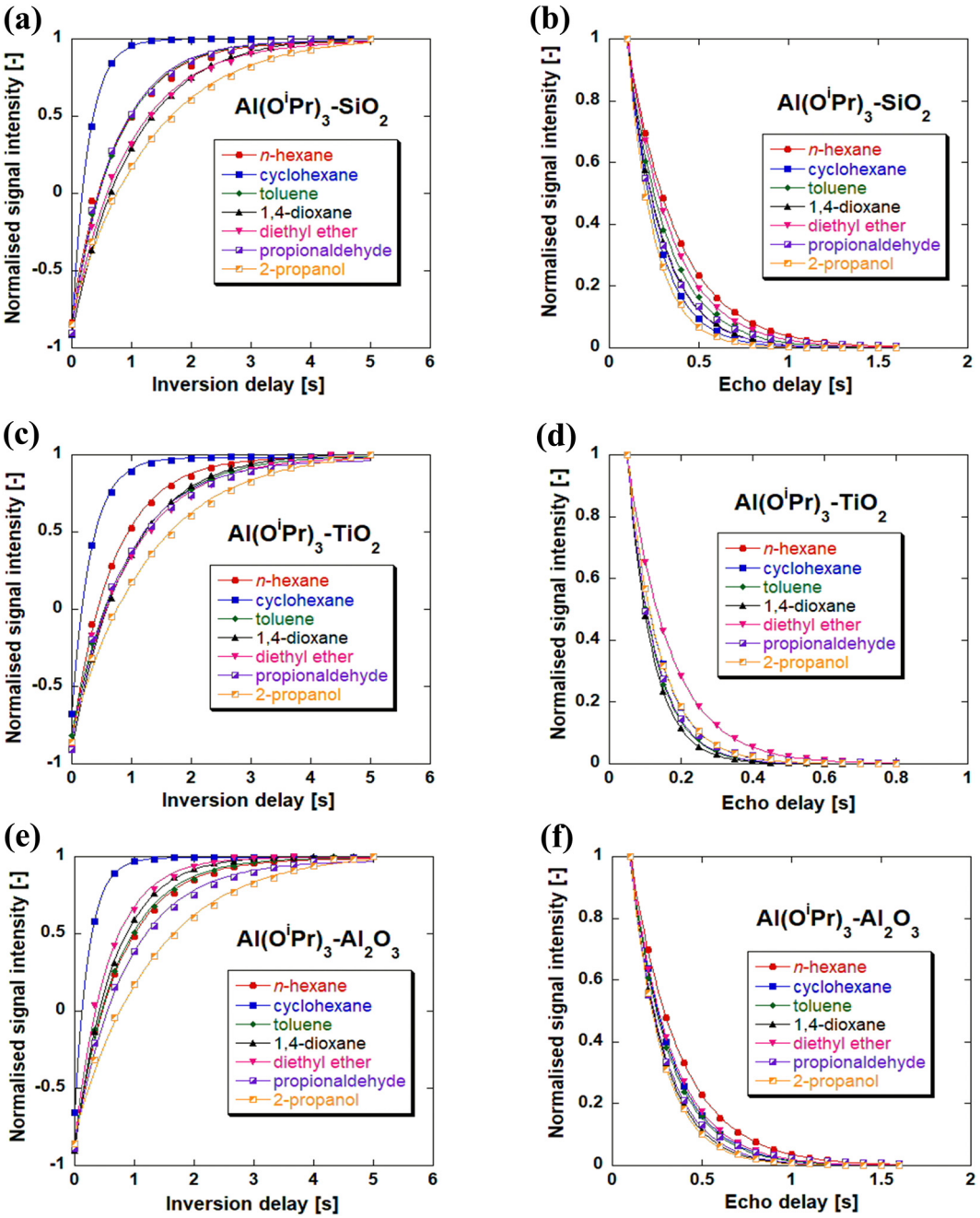

Fig. 3 T_1 relaxation plots for solvents and reactant within (a) Al(O^{i}Pr)$_3$–SiO$_2$, (c) Al(O^{i}Pr)$_3$–TiO$_2$ and (e) Al(O^{i}Pr)$_3$–Al$_2$O$_3$. T_2 CPMG plots for solvents and reactants within (b) Al(O^{i}Pr)$_3$–SiO$_2$, (d) Al(O^{i}Pr)$_3$–TiO$_2$ and (f) Al(O^{i}Pr)$_3$–Al$_2$O$_3$.

surface interactions. The spin-lattice relaxation (longitudinal relaxation) T_1, was measured by the inversion recovery pulse sequence while spin–spin relaxation time (transverse relaxation) T_2, was measured using the CPMG pulse sequence.[30] Experimental plots of T_1 and T_2 relaxation measurements are presented in Fig. 3 for the heterogenised catalysts utilised in this study. Fig. 3 displays the T_1 inversion recovery (a, c, e) and T_2 CPMG decays (b, d, f). More information on the experimental plots of T_1 and T_2 of the various supports can be found in Fig. S1 of the ESI.†

Table 3 reports the values of the T_1/T_2 ratio for different solvents and reactants in the heterogenised catalysts studied. Individual values of T_1 and T_2 can be found in Tables S10–S12 of the ESI.† The values of the ratio of T_1/T_2 for the supports in both solvents and reactants are observed to decrease after functionalisation with Al(O^{i}Pr)$_3$.

Comparing the data of Fig. 2 and Table 3, lower yields are observed in solvents with much higher T_1/T_2 values than the reactants propionaldehyde and 2-propanol, such as 1,4-dioxane (yield in the range of 35–36% for the three catalysts) and diethyl

Table 3 T_1/T_2 relaxation of the solvents and reactants in $Al(O^iPr)_3$–SiO_2, $Al(O^iPr)_3$–TiO_2 and $Al(O^iPr)_3$–Al_2O_3. The relative error on T_1/T_2 is in the range of 3–5%

Entry	Solvent	Catalyst	T_1/T_2
1.	*n*-Hexane	$Al(O^iPr)_3$–SiO_2	2.7
2.	*n*-Hexane	$Al(O^iPr)_3$–TiO_2	2.9
3.	*n*-Hexane	$Al(O^iPr)_3$–Al_2O_3	2.8
4.	Cyclohexane	$Al(O^iPr)_3$–SiO_2	3.2
5.	Cyclohexane	$Al(O^iPr)_3$–TiO_2	3.7
6.	Cyclohexane	$Al(O^iPr)_3$–Al_2O_3	3.7
7.	Toluene	$Al(O^iPr)_3$–SiO_2	4.0
8.	Toluene	$Al(O^iPr)_3$–TiO_2	4.2
9.	Toluene	$Al(O^iPr)_3$–Al_2O_3	4.1
10.	1,4-Dioxane	$Al(O^iPr)_3$–SiO_2	5.3
11.	1,4-Dioxane	$Al(O^iPr)_3$–TiO_2	5.4
12.	1,4-Dioxane	$Al(O^iPr)_3$–Al_2O_3	5.3
13.	Diethyl ether	$Al(O^iPr)_3$–SiO_2	7.8
14.	Diethyl ether	$Al(O^iPr)_3$–TiO_2	8.0
15.	Diethyl ether	$Al(O^iPr)_3$–Al_2O_3	7.9
16.	Propionaldehyde	$Al(O^iPr)_3$–SiO_2	2.5
17.	Propionaldehyde	$Al(O^iPr)_3$–TiO_2	2.3
18.	Ppropionaldehyde	$Al(O^iPr)_3$–Al_2O_3	3.1
19.	2-Propanol	$Al(O^iPr)_3$–SiO_2	3.0
20.	2-Propanol	$Al(O^iPr)_3$–TiO_2	3.0
21.	2-Propanol	$Al(O^iPr)_3$–Al_2O_3	3.0

ether (yield in the range of 30–33% for the three catalysts), while much higher yields are observed in solvents with similar T_1/T_2 values as the reactants, as in the case of *n*-hexane (yield in the range of 81–88% for the three catalysts), cyclohexane (yield in the range of 68–73% for the three catalysts) and toluene (yield in the range of 56–59% for the three catalysts).

Fig. 4 reports a plot of the T_1/T_2 ratio *vs.* TOF for the different heterogenised catalysts used in the reaction under study in different solvents. The findings in Fig. 4 show that solvents with higher T_1/T_2, and consequently a stronger surface affinity, result in reduced reactivity, as shown by the findings observed over other heterogeneous[19] and heterogenised catalysts.[49,50] Oxygenated solvents such as 1,4-dioxane and, in particular, diethyl ether are found to exhibit higher adsorption energies compared to linear ones such as alkanes, as suggested by the higher T_1/T_2, see Table 3. A previous study has reported that the diffusion of 1,4-dioxane in porous TiO_2 is influenced by interactions with the surface of the catalyst pores, which is attributed to the lone electron pairs on the oxygen atoms of 1,4-dioxane, which makes the molecule to act as a Lewis base when in contact with the solid surface.[51] This agrees well with the findings reported here. In particular, H-bonding interactions with surface hydroxyls may play an important role, that is, the absence of H-bonding interactions between alkane solvents and the solid surface, which results in a lower T_1/T_2, can promote stronger interactions with the reactants,

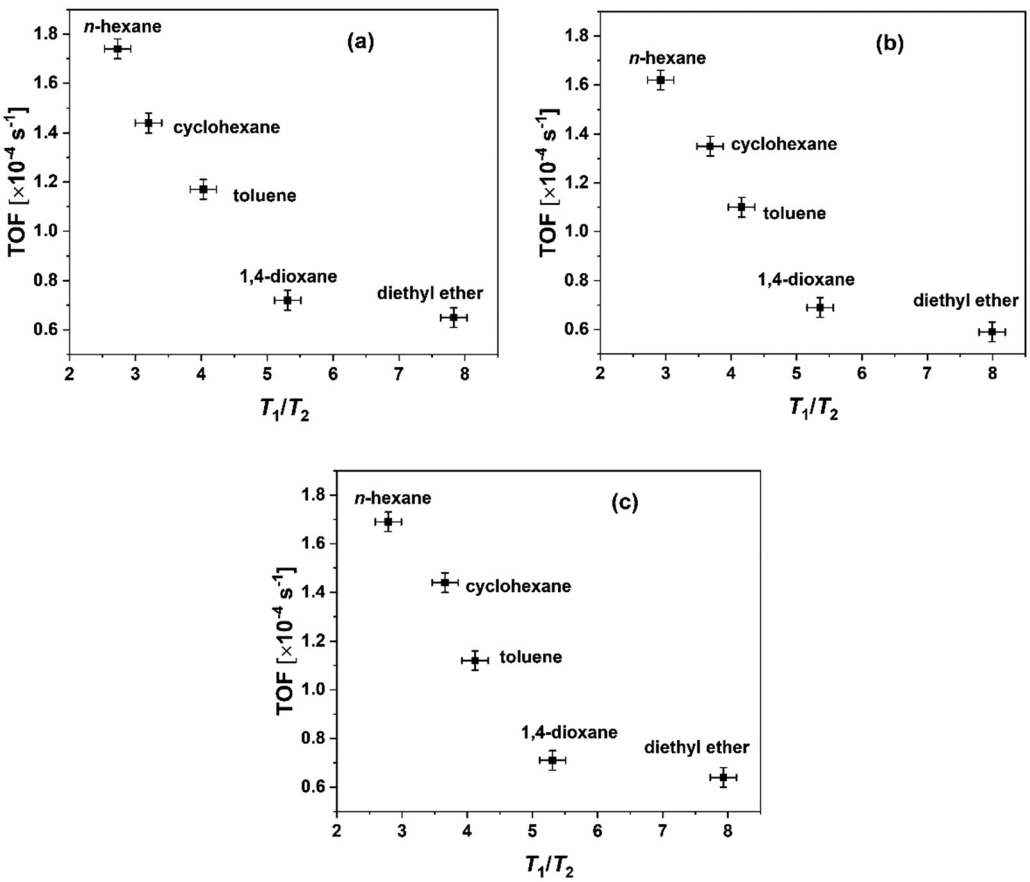

Fig. 4 TOF of the heterogenised catalysts *versus* T_1/T_2 of the various solvents within the catalyst (a) $Al(O^iPr)_3$–SiO_2 (b) $Al(O^iPr)_3$–TiO_2 (c) $Al(O^iPr)_3$–Al_2O_3.

including 2-propanol, hence boosting chemical reactivity at the surface.

From Fig. 4 it is possible to observe as the oxygenated solvents have a stronger surface adsorption capacity compared to hydrocarbons and that this affects catalyst performances. However, given that a similar trend is observed also with the homogenous catalyst in the presence of the same solvent, whereby adsorption over surfaces is neglected, it is reasonable to assume that other types of solvent effects are present, which as previously mentioned, are attributed to the stabilisation of the transition state and solvation effects around the active site. In order to investigate bulk solvation effects, MD studies were carried out, which are presented in the next session.

3.3. MD Results

MD calculations were carried out to better understand solvation effects and accessibility to the catalyst active centre by looking at three different aspects: (i) hydrogen bonding; (ii) interaction energies; (iii) radial distribution function. The structures of each component in the calculation are listed in Table 4 and hydrogen bond donors and acceptors in different components are shown in Table 5.

Hydrogen bonding is a strong intermolecular force, and hydrogen bonds between reactants and catalysts can improve accessibility to reactants to the catalyst active centre. In addition, hydrogen bonding interactions between different species in the system might also affect solvation and aggregation of species.

Table 4 Structure of each component

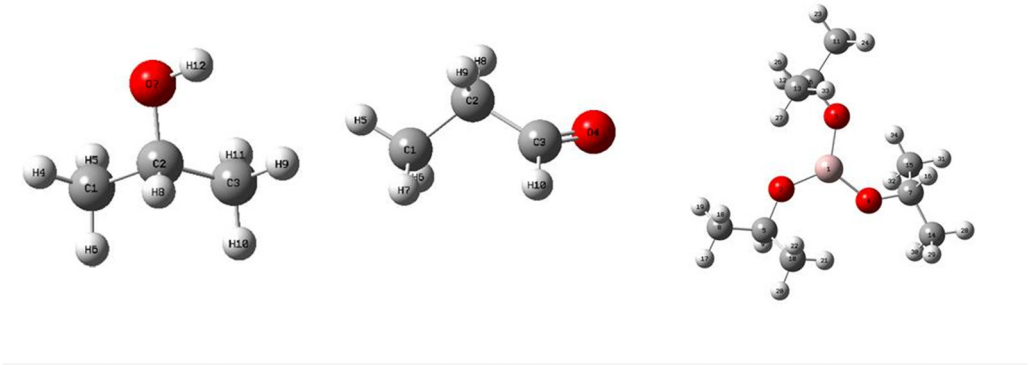

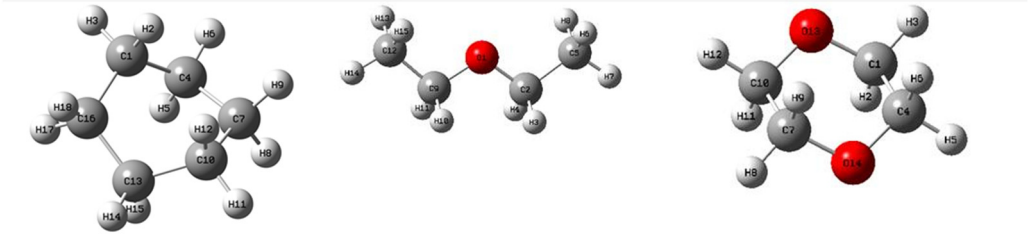

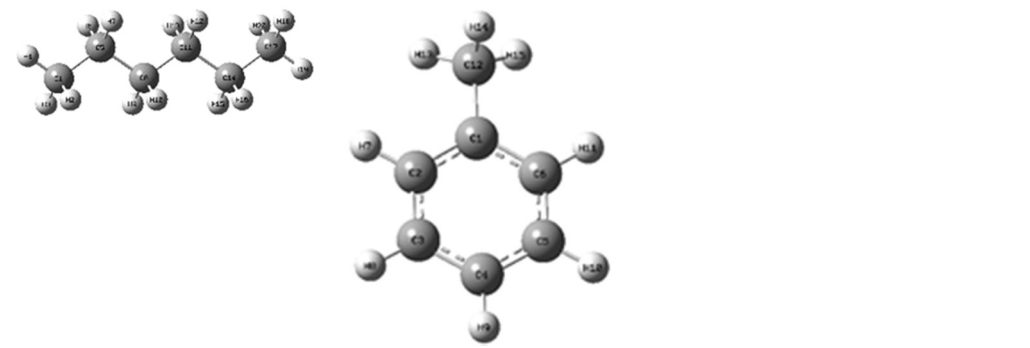

Table 5 Hydrogen bond donors and acceptors in different components

	Propionaldehyde	2-Propanol	Aluminium isopropoxide	Diethyl ether	1,4-Dioxane
Donor-H	—	O7–H12	—	—	—
Acceptor	O4	O7	O2, O3, O4	O1	O13, O14

The average number of hydrogen bonds formed in systems were calculated and are listed in Table 6 using the following geometrical H-bond criteria: donor–acceptor distance less than 3.5 Å and H-donor–acceptor angle no more than 30°. Hydrogen bonding lifetime was calculated as the average over all auto-correlation functions of the existence functions (either 0 or 1) of all H-bonds:

$$C(\tau) = \langle s_i(t) s_i(t+\tau) \rangle \quad (1)$$

with s_i (t) = {0, 1} for H-bond i at time t. The average H-bond lifetime τ can be estimated by the integral of $C(\tau)$:

$$\tau = \int_0^\infty C(\tau) \mathrm{d}\tau \quad (2)$$

From Table 6, H-bonds are only present between 2-propanol (working as both H-bond acceptor and donor) and propionaldehyde, aluminium isopropoxide and the solvents 1,4-dioxane and diethyl ether due to the presence of H-bond acceptors (as shown in Table 5). As expected, the solvents *n*-hexane, cyclohexane and toluene do not form H-bonds with the reactant 2-propanol since they do not have H-bond acceptor groups. When looking at hydrogen bonding interactions between the propionaldehyde and 2-propanol reactants, pALD-PPN, the highest average number of H-bonds between the two species occurs when *n*-hexane and cyclohexane are used as solvents, followed by toluene. Fig. 5 shows the H-bonds when cyclohexane is the solvent of choice. Conversely, when 1,4-dioxane and diethyl ether are used as the solvent, a lower number of H-bonds in propionaldehyde/2-propanol and 2-propanol/aluminium isopropoxide is observed. This may be explained by the ability of 1,4-dioxane and diethyl ether to act as H-bond acceptors, and hence form H-bonds with 2-propanol, the only hydrogen donor. This disrupts interactions between propionaldehyde and 2-propanol. Similarly, average numbers of H-bond interactions between the 2-propanol reactant and the aluminium isopropoxide catalyst, PPN-Catalyst, also show the same trend, that is, lower in 1,4-dioxane and diethyl ether. The difference is clear when comparing alkane species (*n*-hexane, cyclohexane and toluene) with oxygenated species (1,4-dioxane and diethyl ether).

Table 6 Average numbers of hydrogen bonds in different systems

Solvent	pALD-PPN	PPN-Catalyst	PPN-Solvent
1. Cyclohexane	38	8	—
2. Diethyl ether	24	5	76
3. 1,4-Dioxane	14	3	110
4. *n*-Hexane	42	9	—
5. Toluene	28	7	—

*pALD = propionaldehyde, PPN = 2-propanol, catalyst = aluminium isopropoxide ($Al(O^iPr)_3$).

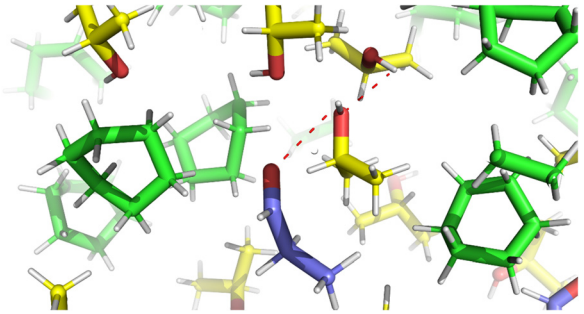

Fig. 5 Visualisation of H-bonds within 2-propanol (carbon: yellow; oxygen: red; hydrogen: white) and between 2-propanol and propionaldehyde (carbon: blue; oxygen: red; hydrogen: white) when using cyclohexane as the solvent (carbon: green; hydrogen: white).

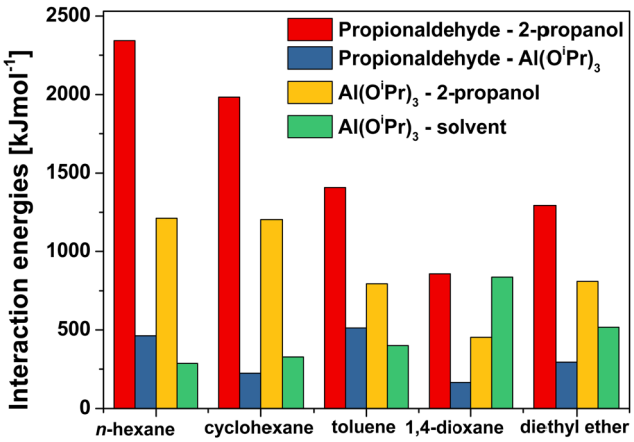

Fig. 6 Interaction energies between reactants (propionaldehyde, 2-propanol), aluminium isopropoxide and solvents in the solvent/reactants/catalyst systems.

In addition to hydrogen bonds, interaction energies between solvents, reactants and the catalyst aluminium isopropoxide were also investigated and shown in Fig. 6.

It is interesting to note that, when interaction energies between solvent and catalysts are considered, solvents such as 1,4-dioxane, diethyl ether and toluene have a stronger interaction with the aluminium catalysts. These results suggest that such solvents might hinder access of reactants to the aluminium centre, hence decreasing the reactivity, which is what has been speculated in previous work on similar systems.[45] The MD results here provide a clear and direct explanation to this phenomenon. Looking at the data in Fig. 6, it is also possible to observe that the energies of interaction between the two reactants,

propionaldehyde and 2-propanol, and those between the catalyst ($Al(O^iPr)_3$) and the reactant 2-propanol, are higher in *n*-hexane and cyclohexane solvents. This indicates that both propionaldehyde and the catalyst have more favourable interactions with 2-propanol in *n*-hexane and cyclohexane, whereas such interactions are less favourable in solvents such as 1,4-dioxane and diethyl ether. This is consistent with the results on hydrogen bonding interactions and again suggests that a more favourable interaction between two reactants and between catalyst and reactants might contribute to a better performance in the reactions.

It is noted that, whilst interaction energy values of 2-propanol – ($Al(O^iPr)_3$) and 2-propanol – propionaldehyde in *n*-hexane and cyclohexane solvents are higher than toluene, the energies between propionaldehyde and ($Al(O^iPr)_3$) in these two solvents are lower than in toluene. This is because a large number of propionaldehyde molecules forming hydrogen bonds with 2-propanol in *n*-hexane and cyclohexane solvents leads to less propionaldehyde around the catalyst.

Finally, in order to understand the distribution of reactant species in the different solvents, the radial distribution functions (RDF) of the centre of mass between the catalyst ($Al(O^iPr)_3$) and the reactant 2-propanol, the catalyst ($Al(O^iPr)_3$) and the reactant propionaldehyde and between the reactants propionaldehyde and 2-propanol in the five solvents were calculated. The radial distribution function (RDF) $g_{AB}(r)$ of A to B can be obtained *via* the following equation:

$$4\pi r^2 g_{AB}(r) = V \sum_{i\in A}^{N_A} \sum_{j\in B}^{N_B} P(r) \quad (3)$$

where, V is the volume, $P(r)$ is the probability of finding a B atom at a distance of r from an A atom.

As shown in Fig. 7, multiple peaks can be identified, indicating the presence of numerous solvent shell layers. Since the first peak imply the nearest molecules in the first solvent shell, here only the first peak is being considered for the analysis. 2-Propanol in the first shell layer of propionaldehyde in cyclohexane is shown in Fig. 8. From Fig. 7 it can be seen that the position of the first peak for the reactant under different conditions is between 0.43 nm and 0.49 nm. It is known to all that the peaks from 0.26 nm to 0.35 nm represent hydrogen bonding, and 0.35–0.50 nm are classified as van der Waals forces.[52–54] As a result, the interaction between the catalyst and the two reactants is mainly attributed to van der Waals forces.

From Fig. 7 it is noted that the higher the peak of species B, the more the species B is arranged in the vicinity of the reference species A, indicating a more favourable interaction between the two species. According to the data in Fig. 7(a), there is a higher density of the reactant 2-propanol around propionaldehyde in cyclohexane and *n*-hexane relative to the

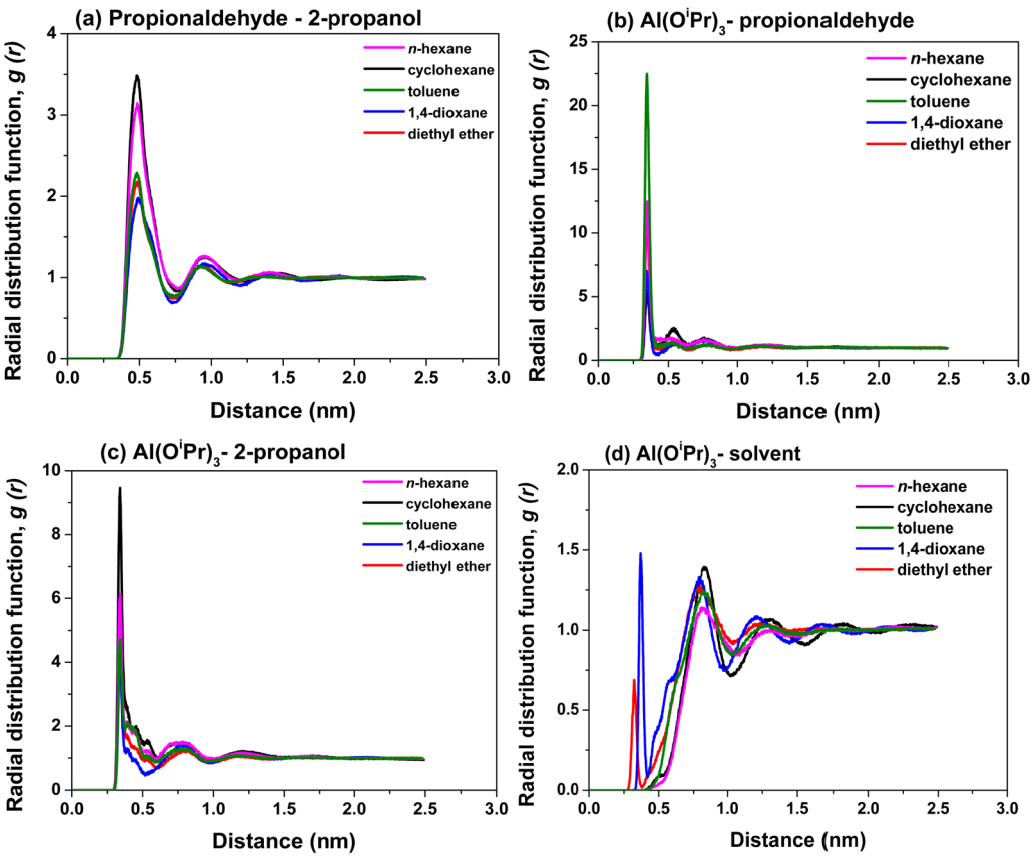

Fig. 7 Centre of mass calculated RDF of (a) propionaldehyde – 2-propanol in different solvents, (b) catalyst – propionaldehyde in different solvents, (c) catalyst – 2-propanol in different solvents and (d) catalyst – solvent for the different solvents.

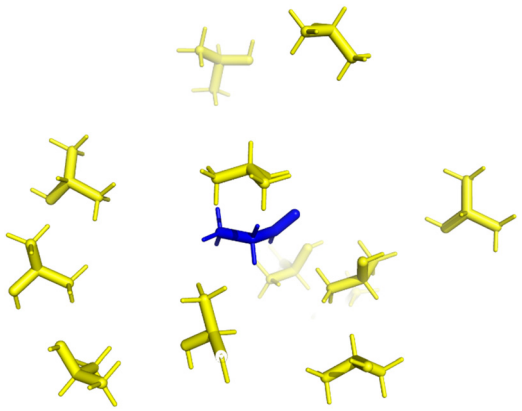

Fig. 8 Distribution of 2-propanol in the first shell layer of propionaldehyde in a cyclohexane box.

other solvents. At the same time, the distribution of the reactant 2-propanol around the catalyst ($Al(O^iPr)_3$) is also more favourable in the same cyclohexane and *n*-hexane solvents, as observed in Fig. 7. Conversely, Fig. 7(b) indicates a more favourable interaction of the reactant propionaldehyde with the catalysts in toluene relative to the other solvents, consistent with the findings in interaction energy. The high density of 1,4-dioxane and diethyl ether around the catalyst may stems from the H-bond forming between 2-propanol and the two solvents. To be more specific, due to H-bond formation, 2-propanol arranges orderly around the catalyst. All of the above findings are again consistent with those on H-bonding interactions as well as interaction energy calculations and in line with our explanation that solvents that favour interactions on the reactant 2-propanol with the catalysts lead to better reaction performances.

In summary, the MD calculation results reported here give new insights at molecular level into solvation effects reported in these systems, giving a comprehensive pictures of the various physical interactions involved in these systems. The results suggest that bulk solvation effects are an important factor in determining reaction performances of these systems, which can be directly linked to the reactivity on the homogeneous systems but are likely to play a role also in the heterogenised systems.

4. Conclusions

Solvent and solvation effects for H-transfer reduction of propionaldehyde to 1-propanol over aluminium isopropoxide grafted on various solid supports was investigated. When compared to homogeneous $Al(O^iPr)_3$ catalysts, the heterogenised catalysts were shown to have similar activity in all solvents, demonstrating that immobilising the homogeneous catalyst onto solid supports is a practical, reliable, and efficient method for this type of reaction.

In order to unravel the reactivity trend in different solvents, NMR relaxation measurements were carried out to study surface affinities of solvents and reactants over the heterogenised catalysts whilst molecular dynamics (MD) was used to study bulk solvation effects. The results reveal that solvents with H-bond accepting ability, such as diethyl ether and 1,4-dioxane, lead to a decrease in catalytic activity, which can be attributed to the ability of such solvents to prevent access to catalytic sites due to solvation effects. In addition, a higher affinity of such solvents for the catalyst surface, as indicated by measurements of the NMR T_1/T_2 ratio, suggest that blocking of active sites immobilised over the surface may also contribute to the reduced catalytic activity. Conversely, solvents such as *n*-hexane and cyclohexane leads to better reaction performances by promoting more favourable interactions between the two reactants and between reactants and catalysts. This work shows that both solvation effects and surface interactions are important factor to consider when immobilising homogeneous catalytic functions on solid support and their knowledge help to rationalise catalytic behaviour and guide design of these catalytic systems.

Data availability

The data that supports the findings of this study are available within the article and the ESI.†

Conflicts of interest

The authors declare that they have no known competing financial interests or personal relationships that could have appeared to influence the work reported in this paper.

Acknowledgements

We would like to thank the Petroleum Technology Development Fund (PTDF) for supporting our research. Carmine D'Agostino and Graziano Di Carmine would also like to acknowledge the EPSRC, grant no. EP/S019138/1. For the purpose of open access, the authors have applied a creative commons attribution (CC BY) licence (where permitted by UKRI, 'open government licence' or 'creative commons attribution no-derivatives (CC BY-ND) licence' may be stated instead) to any author accepted manuscript version arising.

References

1 B. Cornils, W. A. Herrmann, M. Beller and R. Paciello, *Applied homogeneous catalysis with organometallic compounds. a comprehe*, John Wiley & Sons, 2017.
2 A. Corma, M. E. Domine and S. Valencia, Water-resistant solid Lewis acid catalysts: Meerwein–Ponndorf–Verley and Oppenauer reactions catalyzed by tin-beta zeolite, *J. Catal.*, 2003, **215**(2), 294–304.
3 M. Boronat, A. Corma and M. Renz, Mechanism of the Meerwein – Ponndorf – Verley – Oppenauer (MPVO) redox equilibrium on Sn- and Zr – Beta zeolite catalysts, *J. Phys. Chem. B*, 2006, **110**(42), 21168–21174.

4 E. J. Creyghton, S. D. Ganeshie, R. S. Downing and H. Van Bekkum, Stereoselective Meerwein–Ponndorf–Verley and Oppenauer reactions catalysed by zeolite BEA, *J. Mol. Catal. A: Chem.*, 1997, **115**(3), 457–472.

5 A. Koreniuk, K. Maresz and J. Mrowiec-Białoń, Supported zirconium-based continuous-flow microreactor for effective Meerwein–Ponndorf–Verley reduction of cyclohexanone, *Catal. Commun.*, 2015, **64**, 48–51.

6 H. M. Marçon and J. C. Pastre, Continuous flow Meerwein–Ponndorf–Verley reduction of HMF and furfural using basic zirconium carbonate, *RSC Adv.*, 2022, **12**(13), 7980–7989.

7 B. U. Karatas, B. S. Oksal and E. Karatas, New $In(OiPr)_3$-MCM-41 heterogeneous catalyst in MPV reductions of unsaturated carbonyl compounds: effect of mesoporous SBA-15 and MCM-41 as supporting surfaces on catalytic activity of $In(OiPr)_3$, *J. Inclusion Phenom. Macrocyclic Chem.*, 2017, **87**(1–2), 85–94.

8 B. Uysal and B. S. Oksal, New heterogeneous $B(OEt)_3$-MCM-41 catalyst for preparation of α,β-unsaturated alcohols, *Res. Chem. Intermed.*, 2015, **41**(6), 3893–3911.

9 H. Yoshida, Y. Onodera, S. I. Fujita, H. Kawamori and M. Arai, Solvent effects in heterogeneous selective hydrogenation of acetophenone: Differences between Rh/C and Rh/Al_2O_3 catalysts and the superiority of water as a functional solvent, *Green Chem.*, 2015, **17**(3), 1877–1883.

10 A. Muhammad, A. Ismaila, J. Usman, D. Carmine and C. D. Agostino, Activity and stability studies of H-transfer reduction reactions of aldehydes and ketones over aluminium isopropoxide heterogenised catalysts †, *RSC Adv.*, 2022, **12**(52), 33970–33980.

11 C. F. de Graauw, J. A. Peters, H. van Bekkum and J. Huskens, Meerwein–Ponndorf–Verley Reduction and Oppenauer Oxidations, *Synthesis*, 1994, (10), 1007.

12 T. Ooi, T. Miura and K. Maruoka, Highly efficient, catalytic Meerwein–Ponndorf–Verley reduction with a novel bidentate aluminum catalyst, *Angew. Chem., Int. Ed.*, 1998, **37**(17), 2347–2349.

13 R. Anwander, C. Palm, G. Gerstberger, O. Groeger and G. Engelhardt, Enhanced catalytic activity of MCM-41-grafted aluminium isopropoxide in MPV reductions, *Chem. Commun.*, 1998, 1811–1812.

14 M. A. Aramendía, V. Borau, C. Jiménez, J. M. Marinas and F. J. Romero, The Meerwein–Ponndorf–Verley–Oppenauer reaction between 2-hexanol and cyclohexanone on magnesium phosphates, *Catal. Lett.*, 1999, **58**(1), 53–58.

15 B. Uysal, Y. Aksu and B. S. Oksal, Chemoselective reduction of α,β-unsaturated aldehydes and ketones over mesoporous $B(OiPr)_3$-MCM-41 catalyst via MPV reduction process: Preparation, characterization and catalytic application, *J. Porous Mater.*, 2013, **20**(1), 115–127.

16 Y. Zhu, S. Jaenicke and G. K. Chuah, Supported zirconium propoxide – A versatile heterogeneous catalyst for the Meerwein–Ponndorf–Verley reduction, *J. Catal.*, 2003, **218**(2), 396–404.

17 M. A. Isaacs, N. Robinson, B. Barbero, L. J. Durndell, J. C. Manayil and C. M. A. Parlett, *et al.*, Unravelling mass transport in hierarchically porous catalysts, *J. Mater. Chem. A*, 2019, **7**(19), 11814–11825.

18 L. Gilbert and C. Mercier, Solvent effects in heterogeneous catalysis: Application to the synthesis of fine chemicals, *Stud. Surf. Sci. Catal.*, 1993, **78**(C), 51–66.

19 C. D'Agostino, G. L. Brett, P. J. Miedziak, D. W. Knight, G. J. Hutchings and L. F. Gladden, *et al.*, Understanding the solvent effect on the catalytic oxidation of 1,4-butanediol in methanol over Au/TiO_2 catalyst: NMR diffusion and relaxation studies, *Chem. – Eur. J.*, 2012, **18**(45), 14426–14433.

20 C. D'Agostino, M. D. Mantle, L. F. Gladden and G. D. Moggridge, Prediction of mutual diffusion coefficients in non-ideal mixtures from pulsed field gradient NMR data: Triethylamine-water near its consolute point, *Chem. Eng. Sci.*, 2012, **74**, 105–113.

21 A. P. Abbott, C. D'Agostino, S. J. Davis, L. F. Gladden and M. D. Mantle, Do group 1 metal salts form deep eutectic solvents?, *Phys. Chem. Chem. Phys.*, 2016, **18**(36), 25528–25537.

22 T. Lu, K. Zeng, P. Jiang, B. Zhou and R. Xu, Competitive adsorption in CO_2 enhancing shale gas: Low-field NMR measurement combined with molecular simulation for selectivity and displacement efficiency model, *Chem. Eng. J.*, 2022, **440**, 135865.

23 A. T. Krzyzak and I. Habina, Low field ^1H NMR characterization of mesoporous silica MCM-41 and SBA-15 filled with different amount of water, *Microporous Mesoporous Mater.*, 2016, **231**, 230–239.

24 C. D'Agostino, J. Mitchell, M. D. Mantle and L. F. Gladden, Interpretation of NMR relaxation as a tool for characterising the adsorption strength of liquids inside porous materials, *Chem. – Eur. J.*, 2014, **20**(40), 13009–13015.

25 D. Weber, J. Mitchell, J. Mcgregor and L. F. Gladden, Comparing strengths of surface interactions for reactants and solvents in porous catalysts using Two-dimensional NMR relaxation correlations, *J. Phys. Chem. C*, 2009, **113**(16), 6610–6615.

26 C. D'Agostino, S. Chansai, I. Bush, C. Gao, M. D. Mantle and C. Hardacre, *et al.*, Assessing the effect of reducing agents on the selective catalytic reduction of NO_x over Ag/Al_2O_3 catalysts, *Catal. Sci. Technol.*, 2016, **6**(6), 1661–1666.

27 N. Robinson, E. F. May and M. L. Johns, Low-Field Functional Group Resolved Nuclear Spin Relaxation in Mesoporous Silica, *ACS Appl. Mater. Interfaces*, 2021, **13**, 54476–54485.

28 C. D'Agostino, M. R. Feaviour, G. L. Brett, J. Mitchell, A. P. E. York and G. J. Hutchings, *et al.*, Solvent inhibition in the liquid-phase catalytic oxidation of 1,4-butanediol: Understanding the catalyst behaviour from NMR relaxation time measurements, *Catal. Sci. Technol.*, 2016, **6**(21), 7896–7901.

29 M. De Bruyn, D. E. De Vos and P. A. Jacobs, Chemoselective Hydrogen Transfer Reduction of Unsaturated Ketones to Allylic Alcohols with Solid Zr and Hf Catalysts, *Adv. Synth. Catal.*, 2002, **344**(10), 1120–1125.

30 E. Fukushima and S. B. Roeder, Experimental pulse NMR. *A nuts and Holts Approach*, Addison-Wesley, 1981.

31 A. Lindahl and S. Hess van der, *GROMACS 2020 Source code (Version 2020)*, Zenodo, DOI: **10.5281/zenodo.3562495** (accessed: April, 2022).

32 Spoel DVANDER, Lindahl E, Hess B, Groenhof G. GROMACS: Fast, Flexible, and Free. 2005.
33 J. Wang, R. M. Wolf, J. W. Caldwell, P. A. Kollman and D. A. Case, Development and testing of a general Amber force field, *J. Comput. Chem.*, 2004, **25**(9), 1157–1174.
34 P. Li and K. M. Merz, MCPB.py: A Python Based Metal Center Parameter Builder, *J. Chem. Inf. Model.*, 2016, **56**(4), 599–604.
35 M. J. Frisch, G. W. Trucks, H. B. Schlegel, G. E. Scuseria, M. A. Robb and J. R. Cheeseman, *et al.*, *Gaussian 16 Rev. C.01*, Wallingford, CT, 2016.
36 C. I. Bayly, P. Cieplak, W. D. Cornell and P. A. Kollman, A well-behaved electrostatic potential based method using charge restraints for deriving atomic charges: The RESP model, *J. Phys. Chem.*, 1993, **97**(40), 10269–10280.
37 D. A. Case, K. Belfon, I. Y. Ben-Shalom, S. R. Brozell, D. S. Cerutti, T. E. Cheatham, III VWDC, T. A. Darden, R. E. Duke, G. Giambasu, M. K. Gilson, H. Gohlke, A. W. Goetz, R. Harris, S. Izadi, S. A. Izmailov, K. Kasavajhala, A. Kovalenko, R. Krasny, T. Kurtzman, T. S. Lee, S. LeGrand, P. Li, C. Lin JL, T. Luchko, R. Luo, V. Man, K. M. Merz, Y. Miao, O. Mikhailovskii, G. Monard, H. Nguyen, A. Onufriev, F. Pan, S. Pantano, R. Qi, D. R. Roe, A. Roitberg, C. Sagui, S. Schott-Verdugo, J. Shen, C. L. Simmerling, N. R. Skrynnikov, J. Smith, J. Swails, R. C. Walker, J. Wang, L. Wilson, R. M. Wolf, X. Wu, Y. Xiong, D. M. York and P. A. Kollman, *AMBER*, University of California, San Francisco, 2020.
38 D. Case, H. M. Aktulga, K. Belfon, I. Y. Ben-Shalom, J. T. Berryman and S. R. Brozell, *et al.*, *Amber*, University of California, San Francisco, 2021.
39 L. Martínez, R. Andrade, E. Birgin and J. M. Martínez, Software News and Update Packmol: A Package for Building Initial Configurations for Molecular Dynamics Simulations, *J. Comput. Chem.*, 2009, **30**, 2157–2164.
40 G. Bussi, D. Donadio and M. Parrinello, Canonical sampling through velocity rescaling, *J. Chem. Phys.*, 2007, **126**(1), 014101.
41 M. Parrinello and A. Rahman, Polymorphic transitions in single crystals: A new molecular dynamics method, *J. Appl. Phys.*, 1981, **52**(12), 7182–7190.
42 U. Essmann, L. Perera, M. L. Berkowitz, T. Darden, H. Lee and L. G. Pedersen, A smooth particle mesh Ewald method, *J. Chem. Phys.*, 1995, **103**(19), 8577–8593.
43 B. Hess, H. Bekker, H. J. C. Berendsen and J. G. E. M. Fraaije, LINCS: A Linear Constraint Solver for molecular simulations, *J. Comput. Chem.*, 1997, **18**(12), 1463–1472.
44 W. Humphrey, A. Dalke and K. Schulten, VMD: Visual molecular dynamics, *J. Mol. Graphics*, 1996, **14**(1), 33–38, Available from: **https://www.tapbiosystems.com/tap/products/index.htm**.
45 A. Muhammad, G. Di Carmine, L. Forster and C. D'Agostino, Solvent Effects in the Homogeneous Catalytic Reduction of Propionaldehyde with Aluminium Isopropoxide Catalyst: New Insights from PFG NMR and NMR Relaxation Studies, *ChemPhysChem*, 2020, **21**(11), 1101–1106.
46 S. Hübner, J. G. De Vries and V. Farina, Why Does Industry Not Use Immobilized Transition Metal Complexes as Catalysts?, *Adv. Synth. Catal.*, 2016, **358**(1), 3–25.
47 M. J. Kamlet, J. L. Abboud and R. W. Taft, The Solvatochromic Comparison Method. 6. The π* Scale of Solvent Polarities1, *J. Am. Chem. Soc.*, 1977, **99**(18), 6027–6038.
48 A. De Juan, G. Fonrodona and E. Casassas, Solvent classification based on solvatochromic parameters: A comparison with the Snyder approach, *TrAC, Trends Anal. Chem.*, 1997, **16**(1), 52–62.
49 G. Di Carmine, L. Forster, S. Wang, C. Parlett, A. Carlone and C. D'Agostino, NMR relaxation time measurements of solvent effects in an organocatalysed asymmetric aldol reaction over silica SBA-15 supported proline, *React. Chem. Eng.*, 2022, **7**(2), 269–274.
50 G. Di Carmine, D. Ragno, A. Massi and C. D'agostino, Oxidative Coupling of Aldehydes with Alcohol for the Synthesis of Esters Promoted by Polystyrene-Supported N-Heterocyclic Carbene: Unraveling the Solvent Effect on the Catalyst Behavior Using NMR Relaxation, *Org. Lett.*, 2020, **22**(13), 4927–4931.
51 C. D'Agostino, M. D. Mantle and L. F. Gladden, Inhibitory effect of oxygenated heterocyclic compounds in mesoporous catalytic materials: A pulsed-field gradient NMR diffusion study, *Microporous Mesoporous Mater.*, 2018, **269**, 88–92.
52 J. R. Durig, W. N. Kar, C. Zheng and S. Shen, Comparison of *Ab initio* MP2/6-311+G(d,p) predicted carbon–hydrogen bond distances with experimentally determined r0 (C–H) distances, *Struct. Chem.*, 2004, **15**(2), 149–157.
53 T. Steiner and G. R. Desiraju, Distinction between the weak hydrogen bond and the van der Waals interaction, *Chem. Commun.*, 1998, (8), 891–892.
54 X. Fu, X. Fan, X. Ju, X. Qi, J. Li and H. Yu, Molecular dynamic simulations on the interaction between an HTPE polymer and energetic plasticizers in a solid propellant, *RSC Adv.*, 2015, **5**(65), 52844–52851.